Microstructure evolution in helium implanted self-irradiated tungsten annealed at 1700 K studied by TEM

W. Chromiński[1]*, Ł. Ciupiński[1], P. Bazarnik[1], S. Markelj[2], T. Schwarz-Selinger[3]

[1]*Faculty of Materials Science and Engineering, Warsaw University of Technology, Woloska 141, 02-507 Warsaw, Poland*

[2]*Jožef Stefan Institute, Jamova cesta 39, 1000 Ljubljana, Slovenia*

[3]*Max-Planck-Institut für Plasmaphysik, Boltzmannstrasse 2, D-85748 Garching, Germany*

*e-mail: witold.chrominski@pw.edu.pl

Abstract

Tungsten targets have been self-damaged with 20 MeV W^{6+} ions followed by decoration of defects with deuterium and 500 keV helium implantation. Such treatment creates a significant amount of irradiation-induced defects which depend on the distance from the surface. As a final step, selected samples were annealed at 1700 K for 30 min to study defect evolution at high temperature. Detailed TEM analysis, supported with quantification of microstructure, provided an insight into the effect of helium implantation on the previously established dislocation structure and its thermal stability. It was shown that helium is implanted into the material down to approximately 900 nm from the surface and creates a locally enhanced dislocation density which remained stable even after high temperature annealing. This phenomenon is opposite to annihilation of dislocations observed in the sample without helium treatment. At the same time, helium implanted zone is the source of internal stress fields which cover the whole irradiated depth. Thermal treatment releases lattice from this stress. The possible reasons of these occurrences are discussed in the light of helium interactions with vacancies and self-interstitials in the presence of dislocations which directly impacts hydrogen isotopes retention.

Keywords

Radiation damage, tungsten, helium implantation, transmission electron microscopy

1. Introduction

Tungsten is believed to be the most important plasma facing material (PFM) in future fusion reactors. Its combination of physical properties like high melting point, low deuterium retention or high thermal conductivity fits the severe requirements for such application. However, plasma created during the reactor operation directly impacts properties of PFM. Hydrogen isotopes, as the fuel, undergo D-T fusion processes and produce neutrons and helium. Thus, neutron irradiation in the hydrogen-helium plasma – tungsten interactions trigger unavoidable events of complex damaging during the lifetime of

PFMs [1,2]. Since it is impossible to reproduce the conditions prevailing in a fusion environment with fast neutrons in a laboratory, MeV ions are very often used to create displacement damage. Although they cannot replicate neutron irradiation, their interactions with the PFM produce similar defects [3,4]. The process of tungsten ion implantation into tungsten targets is called self-damaging and is considered the best option as it also creates dense cascades and does not alter the composition.

The effect of helium on PFM has been studied by many groups. Due to limited solubility of helium in metals, it tends to form bubbles in the structure of various materials including for example nickel, copper, molybdenum and tungsten [1]. TEM study on the annealing of the helium-loaded polycrystalline tungsten revealed that bubbles are preferably formed close to grain boundaries or dislocations [5]. The former attract helium atoms and allow to create close to equilibrium volumes with dimensions in the range of up to 15 nm. The latter favour very small unstable bubbles which are arranged along the dislocation lines. The temperature rise enables diffusion processes, hence large free surfaces, like grain boundaries, supply bubbles with new atoms and vacancies allowing their growth. Dislocations, which are not efficient diffusion paths for helium, can be decorated with bubbles as a preferred nucleation site [6]. This effect may be beneficial in terms of deuterium retention [7] when the bubbles density is high enough percolating pathways are created for hydrogen isotopes to evacuate to the surface [8]. Additionally, the presence of bubbles at grain boundaries can stabilize them at elevated temperature and suppress recrystallization [9]. Another effect of helium-tungsten interactions is related with the growth of porous nanostructures on the surface, so-called fuzz. It was shown in [10] that under specific exposure conditions (low He energy and high temperature exposure) unstable structures are being formed on the surface of the target and their formation was attributed to the migration of bubbles [11]. Such structures develop in time during annealing, and finally form layer with relatively large (approx. 30 nm) bubbles beneath the surface [12]. Any helium affected structures led to the accelerated degradation of mechanical properties which is undesirable in terms of PFM performance. Additionally, the impact of high temperature cannot be ignored since reactor conditions are complex i.e. plasma and temperature affect PFMs mutually. Depending on the location in the reactor PFMs are exposed to thermal shocks with different intensity. Temperatures close to melting point of the tungsten, can be reached [13]. A combination of temperature shocks and helium dose can lead to another surface damage mechanism – blistering and exfoliation. It is known that there are critical values for these two parameters which cause damaging when exceeded [14]. Blistering may also occur due to the presence of hydrogen isotopes in the plasma with dislocation assisted mechanisms [15]. It was shown that deuterium blisters could be formed only when helium is not present in the plasma [16].

Most of experiments in cited papers were performed on recrystallized tungsten (without irradiation damages), thus there is a scare research data of microstructure investigations focusing on the effect of helium on material with irradiation damages. In [17,18] the influence of He on D transport and retention was studied. He was implanted at 0.5 MeV energy to avoid the surface effects described above and to study the effect the presence of He has in the bulk of tungsten. As this topic is relatively new, it requires detailed microstructure related studies in order to understand how such treatment alter the microstructure of PFM. The main objective of this paper is to support the latter with detailed analysis of microstructural aspects of deuterium loaded self-damaged tungsten subjected to He loading.

2. Experimental

All samples stem from the same batch of hot-rolled polycrystalline tungsten (99.97% wt. at) purchased from Plansee A.G. Initial sample dimensions are $0.8 \times 11.8 \times 15\ mm^3$. Samples were electrochemically polished to a mirror finish. After polishing samples were heated for 2 min in ultra-high vacuum at 2000 K to reduce the intrinsic defect density. After annealing, they were irradiated at room temperature by 20 MeV W ions to a fluence of $7.9\times10^{17}\ W/m^2$ (self-damaging). Samples were mounted on a water-cooled copper holder with a molybdenum mask with dimensions of 10 × 14 mm. The W beam was scanned over this mask opening to achieve a laterally homogenous implantation. Using a displacement energy of 90 eV and evaluating the "vacancy.txt" output for the "Quick calculation of damage" option of the SRIM 2008.04 code one obtains a theoretical peak damage level of 0.23 dpa [19]. In order to decorate the existing traps with D, self-damaged samples were exposed to a well-characterized low-temperature D plasma at 290 K at floating potential which results in an ion energy of < 5 eV/D. A total D fluence of $1.5\times10^{25}\ D/m^2$ was accumulated over 72 h with a constant ion flux to the sample of $6\times10^{19}\ D/(m^2s)$. A homogenous D depth profile within the 2 μm depth with a D concentration of nearly 2 at. % was produced.

After W irradiation and D plasma exposure He irradiation was done with the same setup as the W implantation was done before. 500 keV He ions were implanted at room temperature with a fluence of $7.0\times10^{20}\ He/m^2$. The beam was scanned over the sample surface to achieve a laterally homogenous implantation. The sample was in this case mounted with a molybdenum mask with an opening of 10 × 7.5 mm, meaning only half of the sample was irradiated by He and the second half served as a reference. According to SRIM calculations (Fig. 1) this procedure leads to a He peak concentration of 3.4 at. % in a depth of 0.84 μm with a full width at half maximum of 0.29 μm, creating additional damage of 0.6 dpa at the damage peak in a depth of 0.76 μm. Based on the dislocation appearance revealed during microscopic observations, discussed in this paper, helium affected zone is divided into two sub-regions. The first – track region (TR) named following Debelle`s nomenclature [20] is from the surface down to 680 nm and features low additional damage caused by incoming He ions. The second, helium implanted zone (HIZ) is from 680 to approx. 930 nm depth, contains the most of implanted He. Detailed experimental irradiation procedure and the reasoning for it is described in [17,18].

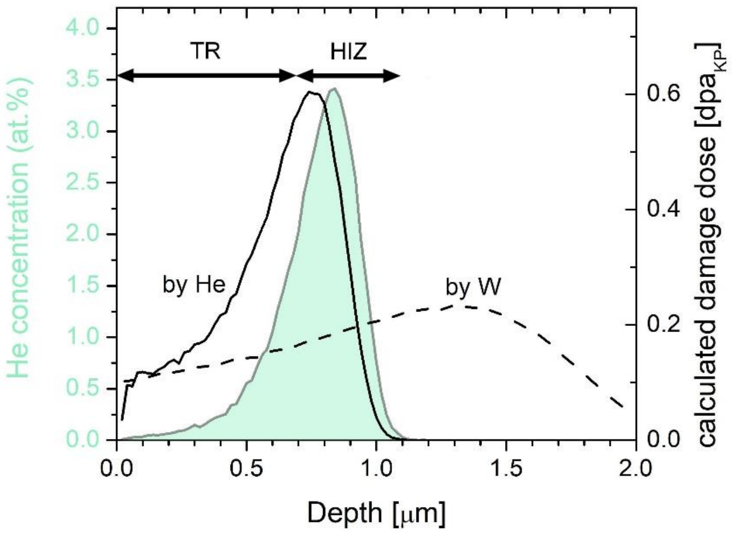

Figure 1 Results of SRIM calculations presenting expected He concentration changes through the depth and displacement damage caused by tungsten self-implantation and He exposure. Black solid line and dashed line show the created displacement damage profile and grey line with green filled area shows the He concentration distribution. Double-arrows indicate the two sub-regions in helium affected zone: track region (TR) and helium implanted zone (HIZ)

After the W and He irradiation two sets of samples were produced for transmission electron microscope (TEM) analysis. The first were self-damaged and helium loaded at room temperature. The second set was treated with the same procedure as before but followed with 30 min 1700 K annealing in ultra-high vacuum. The samples were then cut into half by a diamond saw and each half of the sample was subjected to microstructural studies. Observations were done on the cross sections of irradiated areas cut perpendicularly to the damaged surface. Electron transparent samples were prepared by focus ion beam (FIB) to a thickness of ~300 nm. Acceleration voltage of the beam was set to 40 kV, while the beam current was controlled with the size of aperture depending on the stage of preparation. Then, lamellas were gently thinned by a low energy Ar^+ ion beam system (between 0.6 and 1 keV) to a final thickness of ~100 nm to limit additional defects presence in the microstructure introduced by the FIB beam. General observations were done with the use of Hitachi HD2700 scanning transmission electron microscope (STEM) operated at 200 kV, while detailed dislocations observations were performed with JEOL JEM 1200EX II TEM with acceleration voltage of 120 kV. Observations were carried out after tilting specimens to the closest <001> type zone axis and setting various diffraction conditions. For comparative purposes, only **g**=002 images are presented in this paper. Dislocation densities were estimated with the use of the line intercept method. The number of dislocation line intersections (n) with the array of lines of known length (l) were calculated. The FIB specimen thickness (t) was estimated by setting the sample edge-on in the microscope after the preparation procedures. Dislocation density ρ was calculated with the formula:

$$\rho = \frac{n}{lt}$$

3. Results and discussion

3.1 Microstructure of the sample damaged at RT

Fig. 2(a) shows a STEM image of a typical damaged zone near the tungsten surface created by 20 MeV ions irradiation. Similarly to our previous studies on analogously damaged material [21,22], the depth of the damaged zone is close to 2 μm in accordance with the expectation from the SRIM calculation (see Figure 1). The damaged area is filled with relatively dense dislocations with a uniform distribution. Fig. 2(b) is a STEM image of material subjected to the same self-damage procedure but with subsequent 500 keV helium ion irradiation. The helium affected zone (down to 930 nm) features variances in dislocations appearance through the depth. (quantification provided in Fig. 4). The TR, near the surface, features a visibly lower dislocation density which increases when approaching the interlayer boundary through HIZ. This is visible as a thick dark contour of horizontal orientation. Below this boundary, the dislocation density decreases rapidly. Only tungsten ions induced damage (self-damage) is present there. The total depth of W-ions damaged layer is close to 2 μm like in the sample presented in Fig. 2(a).

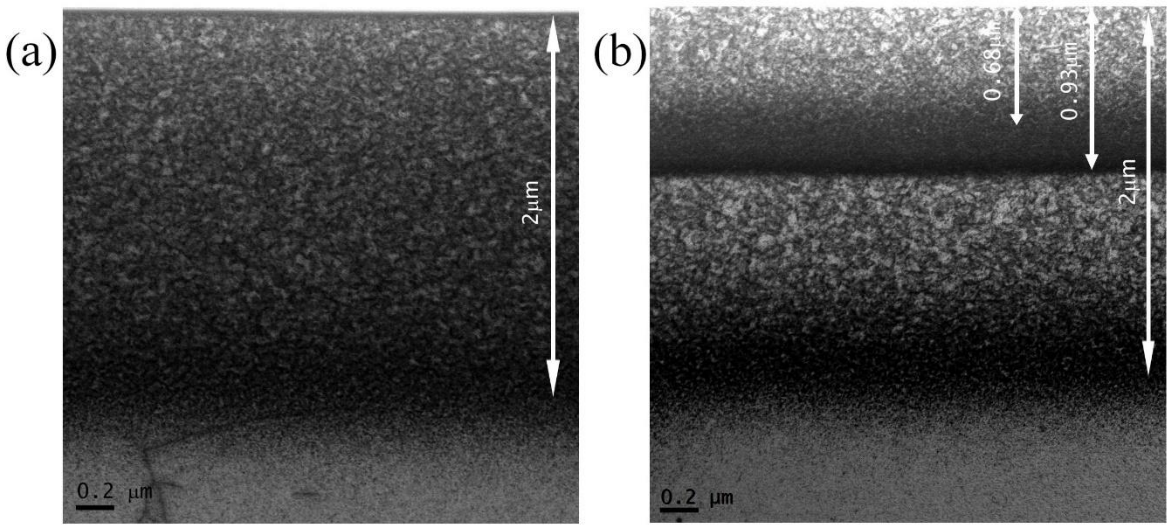

Figure 2 STEM images of W samples implanted at room temperature (a) self-damaged (b) self-damaged followed with 500 keV helium implantation. Helium affected zone can be divided into two sub-regions, as described in text. Trace region 0-0.68 μm and helium implanted zone 0.68-0.93 μm

A different insight into the microstructure is given by TEM which is more sensitive to a local crystal bending thanks to the diffraction contrast. Comparison of microstructural appearance of the two specimens from Fig. 2 is given in Fig. 3. It can be seen that the two investigated samples irradiated under different conditions differ significantly. Fig. 3(a) shows a uniform distribution of dislocations throughout the damaged layer of the self-damaged sample. Dislocations are in the form of short spontaneously arranged lines. It is noteworthy that the background of this image is uniform which indicates no internal stresses in the tungsten matrix after the W ion bombardment. The TEM image of the self-damaged and helium-irradiated sample can be seen in Fig. 3(b). Non-uniform amplitude contrast shades the image, especially in the helium affected zone. The double arrow indicates the helium penetration depth previously inferred from the STEM images. TR, down to 680 nm, is also marked with a double arrow. However, due to contrast variances it is not as clear as in the STEM image. Nevertheless, differences in dislocation densities measured in TR and HIZ are clear in Fig. 4. The boundary between the layers is not so distinct in the TEM image, however it is still noticeable. It can be seen that on the helium side many strain contours separate regions of locally different diffraction conditions. Thus, the visibility of dislocations is limited to local areas where imaging conditions are favorable in this respect. Across relatively small areas of this image, diffraction conditions change several times.

Very high internal stress within the helium affected zone (including TR and HIZ) induced by the strain fields is depicted in Fig. 3(b). The reason for this large strain fields is that at room temperature both vacancies and helium atoms are not likely to travel long distances through the tungsten lattice. The migration energy of single He atoms in tungsten is very low [23,24], the binding force between vacancies and helium atoms is strong [25] what makes it a beneficial condition to form helium-vacancy clusters [23,26]. It was shown in [27] that helium clusters and helium-vacancy complexes do not migrate through tungsten. For this reason, helium trapped in the tungsten lattice has no abilities to travel to dislocations or grain boundaries at room temperature, contrary to what happens at higher temperatures. Displacement damage created by incoming He atoms is characterized by an excess of self-interstitials as they cannot recombine with vacancies that swiftly combine into He-v pairs [28] and are also stabilized by He atoms [29]. Thus, an excess of self-interstitials is present in lattice when compared to materials subjected to displacement damage without the presence of He [29]. According to Hofmann their presence is a direct reason for lattice swelling and inducing lattice stress in samples after the He implantation [28,30]. The strain contour visible in Fig. 3(b) is a direct evidence of the stress presence in He implanted sample. The contour noticed on the helium side continuously passes the boundary between two zones and causes diffraction contrast changes in the W-ions damaged layer as well. However, no additional He damage is expected below HIZ. For this reason, it is believed that stress is transferred from the upper He-affected zone and is spread throughout the W-damaged zone without providing new stress sources.

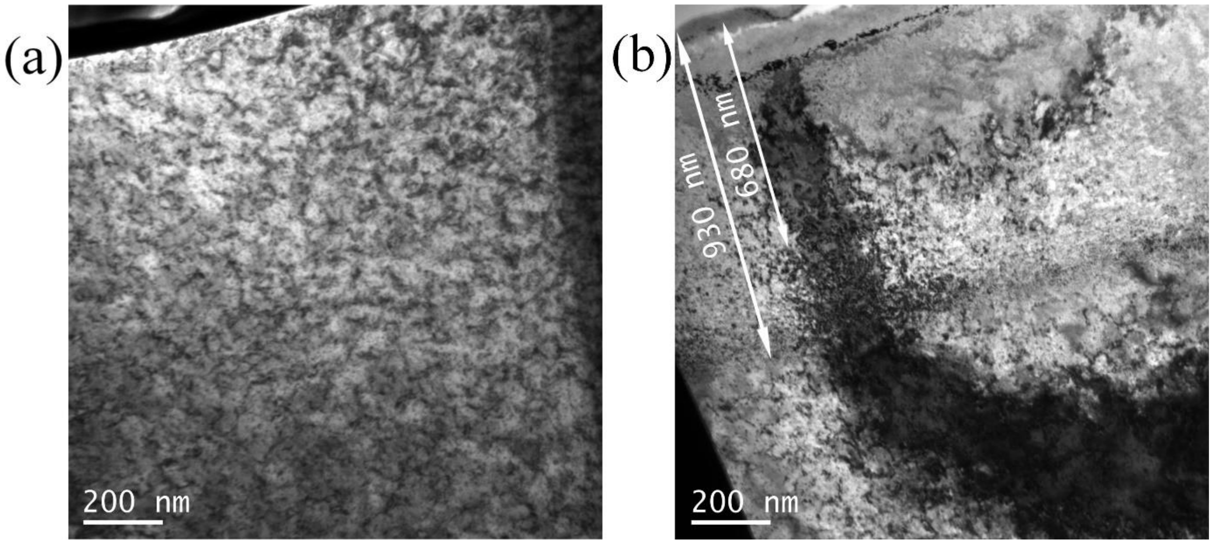

Figure 3 TEM images of samples implanted at room temperature: (a) self-damaged (b) self-damaged followed by helium implantation. Strain contours indicate strong internal stresses.

The comparison of dislocation densities of the investigated samples are shown in Fig. 4. Tungsten self-damaging at RT (blue in the graph) resulted in a dislocation density level in the same order of magnitude as previously observed for samples treated under similar conditions [21,22,31]. Helium ion irradiation caused a significant dislocation density increase, treated at RT. From literature it is known that besides bubble formation incoming energetic helium ions causes displacement damage at low temperatures [27]. Here, the room temperature can promote cascade mechanism of dislocation formation due to lowered vacancy mobility and rather low tendency for thermal dislocation annihilation. The zone below 930 nm, which was not affected by implanted helium atoms maintains a dislocation density at the level of the sample treated with W-ions only, even though the lattice strain produced in the outer zone is transferred to the deeper regions. This observation supports the statement that below 930 nm from the surface no additional helium induced displacement damage exists. We can conclude, that additional damage created by He implantation results in increased dislocation density locally (compare with Fig. 1) within the He implantation zone especially pronounced at the end of range (HIZ) as well as buildup of internal stress even beyond this range.

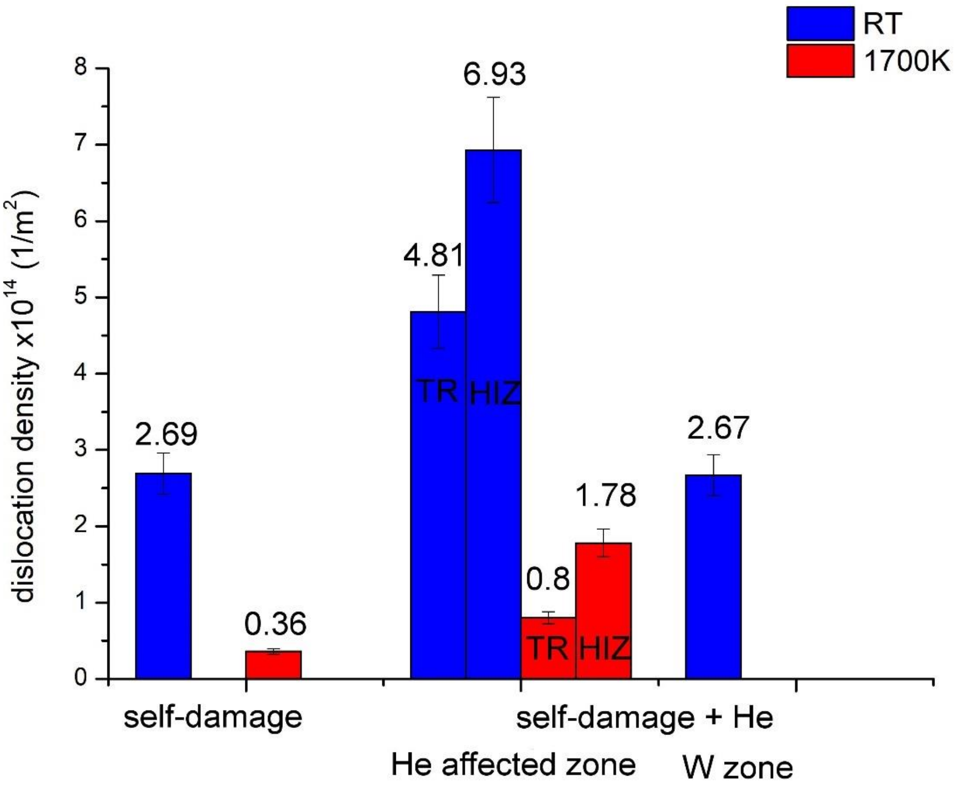

Figure 4 Dislocation densities measured in regions of interest of samples from Figure 1 and 2 (self-damaged and self-damaged followed with helium implantation) as discussed in the text.

Higher magnification TEM images in Fig. 5 allows to compare the appearance of dislocations in the investigated areas of the samples. The self-damaged sample exhibits a uniform distribution of dislocations, as can be seen in Fig. 5(a). Similar structures can be observed in the helium-implanted sample in the deeper, non-helium implanted zone Fig. 5(b). Dislocation lines are spontaneously distributed within the field of view. However, the contrast changes caused by stress transfer from the helium-implanted zone and the dislocation structures visibility criteria cannot be satisfied within the whole field of view. Nevertheless, similar dislocation structures can be observed even in blurred areas of the image.

The dislocation structure in TR and HIZ, Fig. 5(c), was established by self-damaging as a first step and then evolved during helium irradiation. Incoming helium atoms created new vacancies which fragment existing dislocation loops. At the same time, new dislocation lines may be created as reported in the previous works [27,32]. As a result, these two mutual occurrences alter dislocation structures relatively to the self-damaged only. In Fig. 5(d), a magnified area close to the interlayer boundary in HIZ is shown. Arrows indicate few very fine bright spots at the dark background which may be interpreted as helium nanobubbles. The effective thickness of the specimen is reduced there, since He containing bubbles are formed. The electron transparency of the specimen at this location is greater and this very local areas appear brighter even if the background is dark.

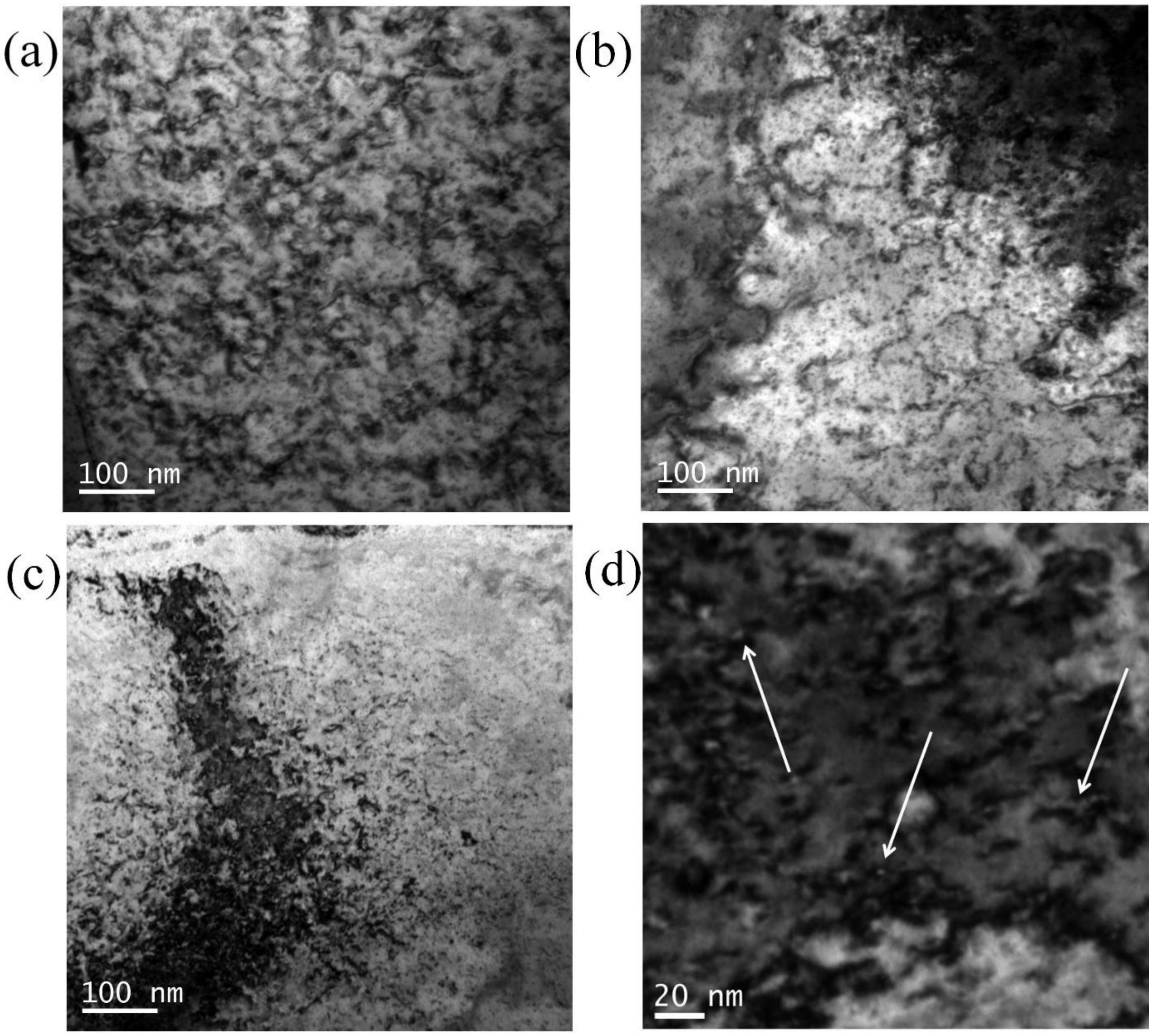

Figure 5 TEM images of samples self-damaged and self-damaged followed by helium implantation at room temperature: (a) self-damaged only (b) helium unaffected zone beyond 930 nm (c) helium affected zone (d) higher magnification of nanobubbles in the helium implanted zone

3.2 Microstructure of the sample damaged at RT and annealed at 1700 K

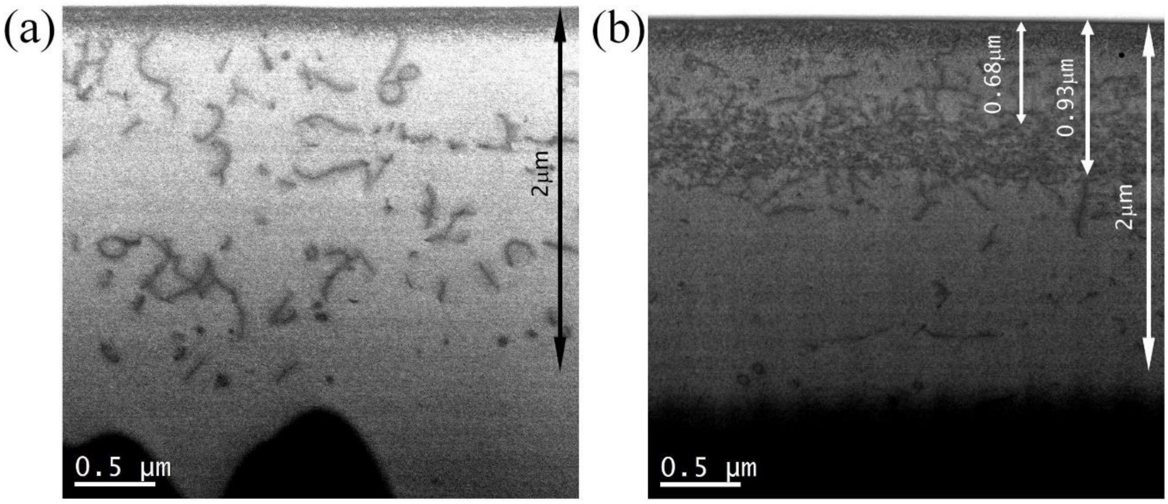

Figure 6 STEM images of samples implanted at room temperature and annealed at 1700K: (a) self-damaged, (b) self-damaged followed with helium implantation

The 1700 K annealing caused significant changes in the irradiated zones. As can be seen in Fig.6(a) which shows a low magnification STEM image, the dislocation structures consist of isolated lines with a spontaneous distribution through the 2 μm depth. The density of defects has decreased significantly (see Fig. 4) as the result of the thermal driven rearrangements. Nevertheless, the 2 μm depth in which dislocations are present suggest that the observed structure resulted from the structures established during the self-irradiation of the sample, as below the indicated zone no dislocations were observed. This observation is consistent with the literature data which indicate accelerated dislocation annihilation at temperature above 1600 K [33]. The annealing of the helium loaded sample resulted in a more complex picture as shown in Fig. 6(b). Defects are mostly accumulated near the inter-layer boundary within HIZ, between 680 and 930 nm. This corresponds well to the location of the calculated additional 0.6 dpa damage caused by He at approximately 760 nm and to the maximum helium concentration at 800 nm from the surface (see Fig. 1). In TR where the implanted He concentration is low, a significantly reduced number of dislocations is present. Comparison of dislocation densities are given in Fig. 4.

The effect of thermally activated rearrangements of dislocation structures in such materials is frequently explained by incorporating neighbouring vacancies from the matrix [33]. This explanation is valid for the sample without helium irradiation and regions of the helium-irradiated sample below HIZ. Negligible amounts of dislocation lines can be observed there (Fig.6 (b)). In the regions close to the inter-boundary layer of helium loaded specimen an increased number of dislocations can be observed which suggest alteration of this mechanism.

The effect of the self-damaging and helium loading procedure on the D retention has been already studied in detail in [17,18]. It was shown there that deuterium gathers mostly at the HIZ about 900 nm beneath the surface of the specimen. The presence of the helium rich zone was linked with so-called trapping of the D near He-vacancy clusters or He bubbles [34]. This effect was linked with the formation of He, D and vacancy clusters within the areas of the highest helium content – close to the 900 nm depth. It was also confirmed by other authors that high temperature annealing does not desorb the helium content from the bulk [34,35]. This means that HIZ with higher density of dislocations at the bottom of helium affected zone (between 680 and 930 nm) still contain helium atoms after the 1700 K treatment [18]. Other studies indicate that elevated temperature may lead to the decoration of dislocation lines with helium bubbles at high temperature [6,36]. However, these studies were performed with in-situ irradiation experiments on thin specimens at high temperature which may lead to thin foil effects which alter the results. In [6] it was discussed that thicker regions of the specimen may feature differences in radiation damages.

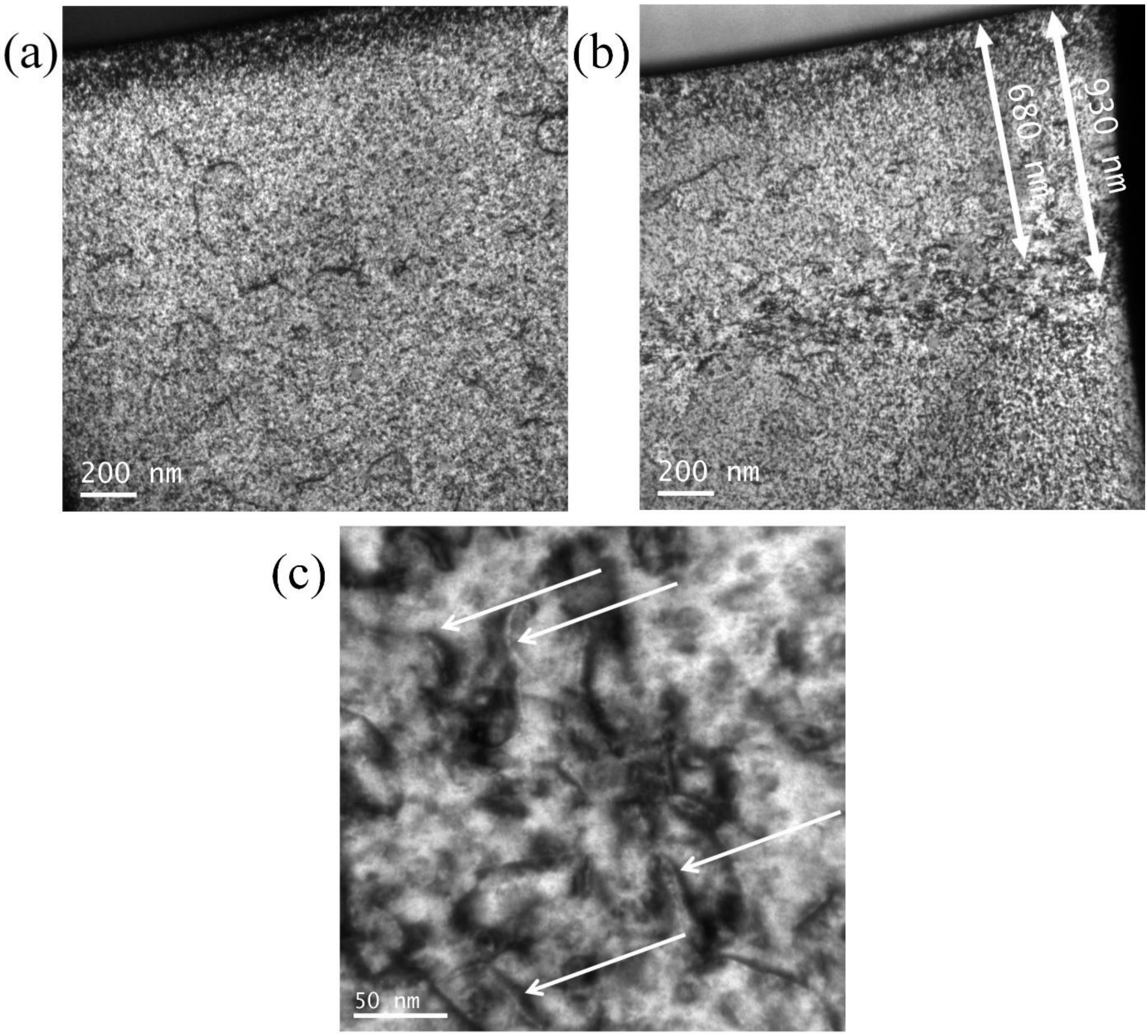

Figure 7 TEM images of samples implanted at room temperature and annealed at 1700 K (a) self-damaged and (b) self-damaged followed with helium implantation, (c) higher magnification of HIZ. Arrows indicate nanobbules attracted by dislocations.

TEM images of damaged layers after 1700 K annealing, presented in Fig. 7, were taken to clarify if the presence of He-bubbles with D atoms can stabilize dislocations during the 1700 K annealing. The background of these images is covered with FIB-induced defects which are the artefacts of this preparation technique. They become clearly visible when reduced number of irradiation defects are present in the matrix. Thus, the noisy appearance of these two images indicates that 1700 K annealing healed most of the previously created defects as well as the strain fields observed before annealing. In Fig. 7(b), an array of dislocations can be noticed in HIZ, approximately 900 nm from the surface. The density of dislocations in this region is significantly higher than in other parts of this sample as well as measured for the sample without helium (Fig. 4). Dislocations present in this zone are in the form of very short segments. A higher magnification image shown in Fig. 7(c) clearly shows that several dislocations appear as visibly brighter lines with some strain contour around, as indicated by arrows. This morphology may be the result of nanobubbles rearrangements caused by a thermal activation.

According to Debelle et al., helium implanted at 500 keV does not desorb during thermal treatment but form bubbles when the fluence during implantation was high enough [34]. The presence of dislocations formed during prior tungsten ions implantation may provide preferential sites for bubbles location upon thermal treatment. Thermally activated motion of dislocations enables collecting spontaneously arranged bubbles and distribute He along dislocation line. As a result, He atoms gather in the form of chains of very fine bubbles along the dislocation line [37]. The change in bubbles appearance in TEM images can be followed in Figs. 5(d) and 7(c). The former shows bubbles which are arranged rather spontaneously within the field of view, while the latter exhibit bubbles arranged along the dislocation lines. Dislocations pinned by bubbles are stable and do not annihilate during the high temperature annealing. Their presence may explain the increased deuterium retention reported in our previous studies [17,18].

The relocation of He atom positions during annealing affects the strain fields observed in samples before annealing, see Figs. 3 and 5. According to Hofmann et al., the strain fields presence in tungsten after He implantation is the result of self-interstitials abundance created by incoming He and W atoms in lattice collisions [28,30]. Presence of implanted He may lead to stabilizing self-interstitials in He-self-interstitial clusters within the lattice at room temperature which act as sources of stress [29]. Thus, when helium atoms rearrange themselves during thermal exposure, self-interstitials regain mobility and annihilate in defect sinks such dislocations or grain boundaries [36,38]. The release of tungsten atoms from interstitials positions reduces the lattice internal strain, as depicted in Fig. 7(b).

4. Summary

STEM and TEM observations have been carried out on samples damaged with 20 MeV tungsten ions followed by 500 keV helium implantation. Helium-irradiation creates an additional disturbance to the lattice down to 930 nm depth from the surface which results in the increased dislocation density and presence of stress fields within damaged zones. After annealing at 1700 K dislocation structures created previously experience significant rearrangements due to thermally activated phenomena. In the regions with the highest helium content dislocations were stabilized due to helium-dislocation interactions which resulted in dislocation lines decorated with very fine nanobubbles. At the same time, regions unaffected with helium feature significantly reduced dislocation densities after the annealing.

Acknowledgements

This work has been carried out within the framework of the EUROfusion Consortium and has received funding from the Euratom research and training programme 2014–2018 and 2019–2020 under Grant agreement No. 633053. The views and opinions expressed herein do not necessarily reflect those of the European Commission.

The Polish authors also acknowledge the financial support from the Polish Ministry of Science and Higher Education, grant no. 5018/H2020-Euratom/2019/2

SM acknowledges the support from the Slovenian Research Agency (research core funding No. P2-0405).

Data availability

The raw data required to reproduce these findings cannot be shared at this time as the data also forms part of an ongoing study.

References

[1] K.D. Hammond, Helium, hydrogen, and fuzz in plasma-facing materials, Mater. Res. Express. 4 (2017) 104002. doi:10.1088/2053-1591/aa8c22.

[2] S. Das, Recent advances in characterising irradiation damage in tungsten for fusion power, SN Appl. Sci. 1 (2019) 1–20. doi:10.1007/s42452-019-1591-0.

[3] G.S. Was, Fundamentals of Radiation Materials Science, 2007. doi:10.1007/978-3-540-49472-0.

[4] O. V. Ogorodnikova, V. Gann, Simulation of neutron-induced damage in tungsten by irradiation with energetic self-ions, J. Nucl. Mater. 460 (2015) 60–71. doi:10.1016/j.jnucmat.2015.02.004.

[5] V.N. Chernikov, J. V Lakhotkin, H. Ullmaier, H. Trinkaus, P. Jung, H.J. Bierfeld, Helium-induced swelling in tungsten during postimplantation annealing, J. Nucl. Mater. 212–215 (1994) 375–381.

[6] X. Yi, K. Arakawa, F. Ferroni, M.L. Jenkins, W. Han, P. Liu, et al., High-temperature damage evolution in 10 keV He+ irradiated W and W-5Re, Mater. Charact. 145 (2018) 77–86. doi:10.1016/j.matchar.2018.08.026.

[7] H. Iwakiri, K. Morishita, N. Yoshida, Effects of helium bombardment on the deuterium behavior in tungsten, J. Nucl. Mater. 307–311 (2002) 135–138.

[8] M. Miyamoto, D. Nishijima, M.J. Baldwin, R.P. Doerner, Y. Ueda, K. Yasunaga, et al., Microscopic damage of tungsten exposed to deuterium – helium mixture plasma in PISCES and its impacts on retention property, J. Nucl. Mater. 415 (2011) S657–S660. doi:10.1016/j.jnucmat.2011.01.008.

[9] W. Guo, L. Cheng, G. De Temmerman, Y. Yuan, G.-H. Lu, Retarded recrystallization of helium-exposed tungsten, Nucl. Fusion. 58 (2018) 106011.

[10] S. Kajita, N. Yoshida, R. Yoshihara, N. Ohno, T. Yokochi, M. Tokitani, et al., TEM analysis of high temperature annealed W nanostructure surfaces, J. Nucl. Mater. 421 (2012) 22–27. doi:10.1016/j.jnucmat.2011.11.044.

[11] S. Kajita, W. Sakaguchi, N. Ohno, N. Yoshida, T. Saeki, Formation process of tungsten nanostructure by the exposure to helium plasma under fusion relevant plasma conditions, Nucl. Fusion. 49 (2009) 095005. doi:10.1088/0029-5515/49/9/095005.

[12] S. Kajita, N. Yoshida, R. Yoshihara, N. Ohno, M. Yamagiwa, TEM observation of the growth process of helium nanobubbles on tungsten : Nanostructure formation mechanism, J. Nucl. Mater. 418 (2011) 152–158. doi:10.1016/j.jnucmat.2011.06.026.

[13] A.R. Raffray, G. Federici, A. Hassanein, D. Haynes, Dynamic chamber armor behavior in IFE and MFE, Fusion Eng. Des. 63–64 (2002) 597–608.

[14] S.B. Gilliam, S.M. Gidcumb, N.R. Parikh, D.G. Forsythe, B.K. Patnaik, J.D. Hunn, et al., Retention and surface blistering of helium irradiated tungsten as a first wall material, J. Nucl. Mater. 347 (2008) 289–297. doi:10.1016/j.jnucmat.2005.08.017.

[15] A. Manhard, L. Gao, Blisters formed by D plasma exposure in an electron-transparent tungsten sample, Nucl. Mater. Energy. 17 (2018) 248–252. doi:10.1016/j.nme.2018.11.014.

[16] V.K. Alimov, W.M. Shu, J. Roth, K. Sugiyama, S. Lindig, M. Balden, et al., Surface morphology and deuterium retention in tungsten exposed to low-energy , high flux pure and helium-seeded

deuterium plasmas, Phys. Scr. T138 (2009) 014048. doi:10.1088/0031-8949/2009/T138/014048.

[17] S. Markelj, T. Schwarz-Selinger, A. Založnik, Hydrogen isotope accumulation in the helium implantation zone in tungsten, Nucl. Fusion. 57 (2017) 064002.

[18] S. Markelj, T. Schwarz-Selinger, M. Pečovnik, W. Chromiński, A. Šestan, J. Zavašnik, Deuterium transport and retention in the bulk of tungsten containing helium: the effect of helium concentration and microstructure, Nucl. Fusion. (2020). doi:10.1088/1741-4326/abadae.

[19] www.srim.org, (n.d.).

[20] A. Debelle, M.F. Barthe, T. Sauvage, First temperature stage evolution of irradiation-induced defects in tungsten studied by positron annihilation spectroscopy, J. Nucl. Mater. 376 (2008) 216–221. doi:10.1016/j.jnucmat.2008.03.002.

[21] J. Grzonka, Ciupiński, J. Smalc-Koziorowska, O. V. Ogorodnikova, M. Mayer, K.J. Kurzydłowski, Electron microscopy observations of radiation damage in irradiated and annealed tungsten, Nucl. Instruments Methods Phys. Res. Sect. B Beam Interact. with Mater. Atoms. 340 (2014) 27–33. doi:10.1016/j.nimb.2014.07.043.

[22] Ł. Ciupiński, O. V. Ogorodnikova, T. Płociński, M. Andrzejczuk, M. Rasiński, M. Mayer, et al., TEM observations of radiation damage in tungsten irradiated by 20 MeV W ions, Nucl. Instruments Methods Phys. Res. Sect. B Beam Interact. with Mater. Atoms. 317 (2013) 159–164. doi:10.1016/j.nimb.2013.03.022.

[23] F. Sefta, K.D. Hammond, N. Juslin, B.D. Wirth, Tungsten surface evolution by helium bubble nucleation, growth and rupture, Nucl. Fusion. 53 (2013) 073015. doi:10.1088/0029-5515/53/7/073015.

[24] K.D. Hammond, D. Maroudas, B.D. Wirth, Theoretical Model of Helium Bubble Growth and Density in Plasma- Facing Metals, Sci. Rep. 10 (2020) 2192. doi:10.1038/s41598-020-58581-8.

[25] C.S. Becquart, C. Domain, Solute – point defect interactions in bcc systems : Focus on first principles modelling in W and RPV steels, Curr. Opin. Solid State Mater. Sci. 16 (2012) 115–125. doi:10.1016/j.cossms.2012.01.001.

[26] C.S. Becquart, C. Domain, Migration Energy of He in W Revisited by Ab Initio Calculations, Phys. Rev. Lett. 97 (2006) 196402. doi:10.1103/PhysRevLett.97.196402.

[27] R.W. Harrison, G. Greaves, J.A. Hinks, S.E. Donnelly, A study of the effect of helium concentration and displacement damage on the microstructure of helium ion irradiated tungsten, J. Nucl. Mater. 495 (2017) 492–503. doi:10.1016/j.jnucmat.2017.08.033.

[28] F. Hofmann, D. Nguyen-Manh, M.R. Gilbert, C.E. Beck, J.K. Eliason, A.A. Maznev, et al.,

Lattice swelling and modulus change in a helium-implanted tungsten alloy: X-ray micro-diffraction, surface acoustic wave measurements, and multiscale modelling, Acta Mater. 89 (2015) 352–363. doi:10.1016/j.actamat.2015.01.055.

[29] A. De Backer, P.E. Lhuillier, C.S. Becquart, M.F. Barthe, Modelling of the implantation and the annealing stages of 800 keV 3He implanted tungsten: Formation of nanovoids in the near surface region, J. Nucl. Mater. 429 (2012) 78–91. doi:10.1016/j.jnucmat.2012.05.024.

[30] S. Das, W. Liu, R. Xu, F. Hofmann, Helium-implantation-induced lattice strains and defects in tungsten probed by X-ray micro-diffraction, Mater. Des. 160 (2018) 1226–1237. doi:10.1016/j.matdes.2018.11.001.

[31] W. Chrominski, L. Ciupinski, P. Bazarnik, S. Markelj, T. Schwarz-Selinger, TEM investigation of the influence of dose rate on radiation damage and deuterium retention in tungsten, Mater. Charact. 154 (2019) 1–6. doi:10.1016/j.matchar.2019.05.028.

[32] R.W. Harrison, H. Amari, G. Greaves, J.A. Hinks, S.E. Donnelly, Effect of He-appm / DPA ratio on the damage microstructure of tungsten, MRS Adv. 42 (2016) 2893. doi:10.1557/adv.2016.385.

[33] F. Ferroni, X. Yi, K. Arakawa, S.P. Fitzgerald, P.D. Edmondson, S.G. Roberts, High temperature annealing of ion irradiated tungsten, Acta Mater. 90 (2015) 380–393. doi:10.1016/j.actamat.2015.01.067.

[34] A. Debelle, M.F. Barthe, T. Sauvage, R. Belamhawal, A. Chelgoum, P. Desgardin, et al., Helium behaviour and vacancy defect distribution in helium implanted tungsten, J. Nucl. Mater. 362 (2007) 181–188. doi:10.1016/j.jnucmat.2007.01.021.

[35] E. Markina, M. Mayer, S. Elgeti, T. Schwarz-Selinger, Influence of MeV helium implantation on deuterium retention in self-ion implanted tungsten, Phys. Scr. T. 159 (2014) 014045. doi:10.1088/0031-8949/2014/T159/014045.

[36] H. Iwakiri, K. Yasunaga, K. Morishita, N. Yoshida, Microstructure evolution in tungsten during low-energy helium ion irradiation, J. Nucl. Mater. 287 (2000) 1134–1138.

[37] K.D. Hammond, F. Ferroni, B.D. Wirth, Simulation of helium behavior near subsurface prismatic dislocation loops in tungsten, Fusion Sci. Technol. 71 (2017) 7–21. doi:10.13182/FST16-110.

[38] T. Matsui, S. Muto, T. Tanabe, TEM study on deuterium-irradiation-induced defects in tungsten and molybdenum, J. Nucl. Mater. 287 (2000) 1139–1143.